J. Astrophys. Astr. (1997) **18**, 57–71

# On the Role of Nonthermal Electrons in EUV and X-ray Line Emissions from Solar Flares

Ranjna Bakaya *Radio Science Division, National Physical Laboratory, New Delhi 110012, India.*

R. R. Rausaria *Council of Distance Education, IGNOU, New Delhi 110016, India.*

Received 1996 February 22; accepted 1996 June 30

**Abstract.** The energy and angular distribution of electrons as a function of column densities initially for monoenergetic and monodirectional electron beams and incidence angles of 0°, 30° and 60° have been studied by combining small angle scattering using analytical treatment with large angle collisions using Monte Carlo calculations. Using these distributions, X-ray and EUV-line flux have been studied as a function of column density. It is observed that the line flux increases with the increase in column density, becoming significant at intermediate column densities where the electron energies and angular distributions have a non-Maxwellian nature.

*Key words.* Solar flares: X-ray, EUV line emission—non thermal particle distribution.

## 1. Introduction

The evaluation of physical parameters in the context of nonthermal as well as thermal flare models have been reported by Batchelor *et al.* (1985, 1989). Batchelor (1990) discussed some additional results of these investigations and its implications on models of Böhme *et al.* (1977). Klein, Trottet & Magnum (1986), Holman, Kundu and Kane (1989) have analysed individual events using temporal, spectral or spatial information in the context of both thermal and nonthermal electron populations. In the nonthermal and thermal models shock wave particle acceleration and thermal conduction fronts are suggested as most straightforward explanations of the burst time behavior. Wilson *et al.* (1990) have analysed VLA observations at 20.7 cm and 91.6 cm and soft and hard X-ray data from the spectrometers aboard the GOES and SMM (HXRBS) spacecraft. It is found that thermal gyroresonance emission is shown to be the most probable process for the preflash emission at 20.7 cm wave-length while the radio and hard X-ray observations during the remainder of the impulsive phase are shown to be consistent with a confined thermal electron population but are more readily explained by the injection of nonthermal electrons. The spectra of the 1980 June 27th event (Lin *et al.* 1981) have shown an emerging thermal component at energies below 40 keV in addition to nonthermal radiation at higher energies. Hamilton & Petrosian (1992) dispute the thermal nature of the low energy component but analysis of data has shown that a

thermal interpretation is the likely one (Emslie, Coffey & Schwartz 1989). Benka & Holman (1994) developed a formalism for analysing high resolution hard X-ray spectra incorporating the coexistence of thermal and nonthermal bremsstrahlung. They also evaluated both the thermal and nonthermal energetics of the 1980 June 27th event and found good agreement with Lin & Johns (1993) for the accelerated electrons.

Hudson *et al* (1994) concluded that the impulsive soft X-ray emission comes from material heated by precipitating electrons at footpoints and evaporating from the deeper atmosphere into the flaring flux tube. Peter *et al.* (1990) have concluded that future EUV spectroscopy experiments on satellites should be a useful diagnostic tool for studying nonthermal bursts in the solar chromosphere.

X-ray emission from solar flares in the spectral range (1–10) keV is usually interpreted as being produced by a thermal plasma at several million degrees of temperature. Further more line emission of these photon energies cannot be explained in terms of isothermal models of flares. Instead multitemperature models have to be postulated (Meekins *et al* 1970; Neupert 1971). For these reasons, it is necessary to investigate ionization and recombination processes which occur in a plasma whose electrons follow a non-Maxwellian energy distribution. The EUV and X-ray line emission for power law electron distributions have been studied by Landini *et al.* (1973), and Haug (1979). However the calculations are for thin target geometry and effects of multiple scattering on electron energy distributions have not been considered. Hard X-ray observations of Kane *et al* (1979) with PVO/ISEE-3 satellites on-board SMM strongly favours the thick target geometry for X-ray generation Hoyang *et al.* (1981).

The electrons accelerated during solar flares travel towards the chromosphere and encounter increasing densities and lose energy in collision with the ambient particles. A fraction of the colliding particle energy is converted into bremsstrahlung X-rays and the rest is given to surrounding medium as heat. Feldman *et al.* (1994) speculated that the small emitting region seen in SXT flare images is a pinched plasma formed by a current that steadily increases with time over the rise part of the flare. This leads to an increase in temperature until a critical point is reached when particles are accelerated to energies of several tens of keV. These escape from the hot plasma, travel down the legs of the flux tube containing the hot plasma and emit high energy ($\geq$ 20 keV) X-ray as they encounter the chromosphere, thus accounting for the impulsive X-ray burst. The current decreases later on, particle acceleration ceases and the heating of the plasma declines and the hot plasma cools by radiation (Feldman *et al.* 1994). Cheng (1990) analysed the UV spectra for the 1974 January 21st flare, in particular those obtained prior to and during impulsive HXR burst and summarized the result that transition region plasma in the flare shows large intensity enhancement and large nonthermal turbulent mass motion velocity of the order of l00 keV $s^{-1}$ before the impulsive hard X-ray burst.

Cheng (1990) found that heating of the preflare plasma to temperatures as high as $10^7$ K stalled before the onset of the impulsive HXR burst. The density of the preimpulsive transition region and chromospheric plasma is already high. Line ratios give a value of $10^{12}$ $cm^{-3}$ for the transition region plasma. The first requirement for a collisional model of flare heating is that the energy carried by nonthermal electrons is sufficient to heat the coronal plasma up to a temperature of

the order of $10^7$ K. Assuming a thick target model for electron bremsstrahlung, a number of authors have shown that the kinetic energy of accelerated electrons is adequate not only to explain the heating of the soft X-ray plasma but also to account for most, if not all, the energy of a solar flare (Cheng 1972; Duijveman *et al.* 1983; Emslie 1983; Brown 1973). Cheng (1972) studied an impulsive homogeneous model in which electrons are instantaneously injected over the whole region and then decay through a collisional process. Syrovatski & Shmeleva (1972) analysed the opposite case of stationary heating by nonthermal electrons injected continuously at the boundary of the absorption region. Giachetti & Pallavicini (1976) have discussed the problem of collisional heating in a more general way for arbitrary source function of accelerated electrons depending both on space and time. Emslie (1978) and Macneice *et al.* (1984) have also studied the heating function and the role of nonthermal electrons for the heating of chromosphere. However the effect of electron source directivity and the dispersion in electron energy and angular distributions about the mean are not included. In this paper, we have incorporated these effects in computations. Electron distribution used in the calculations are given in section 2. Computations of X-ray and EUV flux are given in section 3.

## 2. Electron distributions

Usually the energy spectrum of the nonthermal electrons above l0 keV is taken to be in the form of a power law. We consider initially a monoenergetic incident electron beam, instead of a power law distribution having, energies of 30, 100 and 300 keV. All these incident beams are characterized by a velocity $V$. The components of $V$ in a coordinate system with Z axis are sin $\alpha$ cos $\phi$, sin $\alpha$ sin $\phi$ and cos $\alpha$ where $\alpha$ is the incident angle with respect to vertical direction and becomes the pitch angle in presence of the magnetic field. We consider electrons injected towards the chromosphere at 0°, 30° and 60°. Electron transport has been calculated as a function of height in the atmosphere.

We consider a fully ionized thermal plasma consisting of protons and electrons. It is assumed that the relativistic beam will be influenced only by coulomb forces between the beam electrons and the thermal electrons and protons. For chromospheric and coronal plasma, the mean free path determined by minimum scattering angle is only a fraction of a centimeter, therefore, it is not possible to treat all of the small angle deflection in a pure Monte Carlo procedure. The condensed history of the small angle scattering process treated analytically followed by the Monte Carlo calculations of a single large angle collision process. Details of the calculations are given in Haug *et al.* (1985).

In the condensed history, the numerous collision processes with small energy losses are taken into account by mean energy loss rates. If an electron traverses the distance $d(l)$ in a plasma of electron or proton particle density $n(l)$, its mean loss $dE$ of kinetic energy $E$ by small angle scattering which causes a deviation between the limits $\theta_{\min} < \theta_L$ is given by

$$\overline{dE} = n(l)d(l)\int_{\theta_{\min}}^{\theta_L} \Delta E \frac{\mathrm{d}\sigma}{\mathrm{d}\theta}\,\mathrm{d}\theta, \tag{1}$$

where

$$\Delta E = \frac{-\sin^2\theta}{1-\Gamma^2\cos^2\theta}E$$

$$\Gamma = \left(\frac{\gamma-1}{\gamma+1}\right)^{\frac{1}{2}}. \tag{2}$$

This equation holds for any energy and it refers to the laboratory system where the target electron is initially at rest. For scattering of electrons by protons and electrons, the Born approximation is valid for electron energies $E \geq 1$ keV. In this energy range, the minimum scattering angle (Mott & Massey 1965) is given by

$$\theta_{\min} = \frac{\hbar}{mc\beta\gamma D}, \tag{3}$$

where $h = 2\pi\hbar$ is the planck constant; $m$ the rest mass of the electron and $D$ the maximum impact parameter which usually is supposed to be the Debye length;

$$D = \left(\frac{kT}{4\pi e^2 n}\right)^{\frac{1}{2}} \simeq 6.9\left(\frac{T}{n}\right)^{\frac{1}{2}} \text{cm}, \tag{4}$$

where $k$ is the Boltzman constant; $e$ the electron charge, $T$°K the plasma temperature and n($cm^{-3}$) the particle density. The energy loss according to equation (1) and the mean square value of the angle depend only logarithmically on $\theta_{\min}$. The results are therefore very insensitive to the choice of $\theta_{\min}$. Furthermore, since the knowledge about the temperature and density in the flare plasma is of speculative nature, we take $D = 10(2n)^{-\frac{1}{3}}$. The numerical value of $D$ has been chosen in order that it equals the Debye length for chromospheric heights. Approximating the energy loss according to equation (2) by $\Delta E \simeq E \sin^2\theta$ and using the cross-section (Roy & Reed 1968)

$$d\sigma_R = \frac{2\pi r_0^2}{\beta^4\gamma^2}\frac{\sin\theta}{(1-\cos\theta)^2}\left(1-\beta^2\frac{\sin 2\theta}{2}\right)d\theta, \tag{5}$$

where $r_0$ is the classical radius of electron, $\beta = v/c$, the velocity of beam electron in units of $c$, $\gamma = (1-\beta^2)^{-\frac{1}{2}}$ is the Lorentz factor. It can be seen that the variance for $\theta_L = 1°$ is only 0.06 % of the total variance ($\theta_L = \frac{\pi}{4}$). For $\theta_L = 5°$, the variance would be 1.5% of the total variance ($\theta_L = \frac{\pi}{4}$). Although this value is not high either, we choose $\theta_L = 1°$, since the calculation of large angle scattering by means of the Monte-Carlo method can be achieved with plausible expenditure of computer time for $\theta \geq 1°$. Now it is possible to combine the numerous collisions with small energy losses and scattering angles $\theta_L = 1°$ to a condensed history where only the average energy loss is taken into account. In preliminary investigation (Elwert & Rausaria 1978) this average energy loss has been neglected compared to the energy loss by a single collision with $\theta \geq \theta_L$. When traversing the thermal plasma, the electron will not only lose energy continuously, but it is also deflected continuously from its original direction.

The average column density for collisions with scattering angles between $\theta_L$ and $\theta_{\max}$ corresponding to the mean-free path for large angle scattering is given by

$$\bar{N} = \frac{1}{\sigma},$$

where $\sigma$ is the total cross-section given by

$$\sigma = \int_{\theta_L}^{\theta_{\max}} \mathrm{d}\sigma \cong \frac{4\pi r_0^2}{\beta^4\gamma^2}\,\frac{1}{\theta_L^2}\,. \tag{6}$$

The larger the value of $\theta_L$, the larger is the mean angular deflection and the width of the distribution function.

The aim of our computation is to calculate the energy and angular distribution of electrons at various locations in the outer atmosphere of the sun. It is assumed that the particle density $n$ is a function of parameter $S$. In case of horizontal stratification $S$ is the height in the atmosphere counted positively downward. The initial energy and angular distribution of the electrons is given at $S = 0$, the location of the source of fast electrons. The particle density $n$ will be represented by the barometric law

$$n = n_0 e^{as}. \tag{7}$$

The relation between $S$ and the path length is $S = l \cos\theta$ where $\theta$ is the angle between the electron direction and grad $n$. We first calculate the free path $l$, the electron travels before undergoing the next large-angular scattering (Davis 1963; Berger 1963; Hammersley & Handscomb 1964). If an electron with energy $E(S)$ travels within the angle $\theta$ relative to primary direction of the electron, the vertical path $l$ between the $i$th and $(i + 1)$th collision with scattering angles $\theta \geq \theta_L$ is calculated from the probability distribution

$$\Lambda\,(l, s, \cos\theta) = 1 - e^{-N(l,\,s,\,\cos\theta)\sigma},$$

where

$$N(l, s, \cos\theta) = \int_0^l n_0 e^{a(s+l'\cos\theta)}\,dl' = \frac{n_0 e^{as}}{a\cos\theta}\left(e^{al\cos\theta} - 1\right). \tag{8}$$

$(N)$ is the column density along the mean free path and $\sigma$ is the total cross-section (equation 6). Uniformly distributed random numbers $R(O < R < 1)$ are produced by a random number generator. The free path $l$ corresponds to an end with probability $R$; it is determined by $R = \Lambda(l, s, \cos\theta)$. By solving this equation for $l$, the respective free paths have been determined. The shorter of these two free paths is the free path actually traversed. During the traversal of this path length $l$, the electron loses energy by small-angle deflections and changes its direction by random angle $\theta$ which is obtained according to Moliere-Bethe's theory (Moliere 1948; Bethe 1953), using another random number given by

$$C = \int_0^\theta Q_0(\theta)\mathrm{d}\theta.$$

Where $0 < c < 1$. If the electron under consideration with the initial polar angle $\Theta_i$ relative to the primary direction and the azimuthal angle $\phi_i$ collides with an electron or a proton at a location $(S + l\cos\Theta_i)$, it has reduced energy $E(S + l\cos\Theta_i)$ according to equation

$$E[n(l)] = G + \sqrt{G^2 + 2mc^2G}, \tag{9}$$

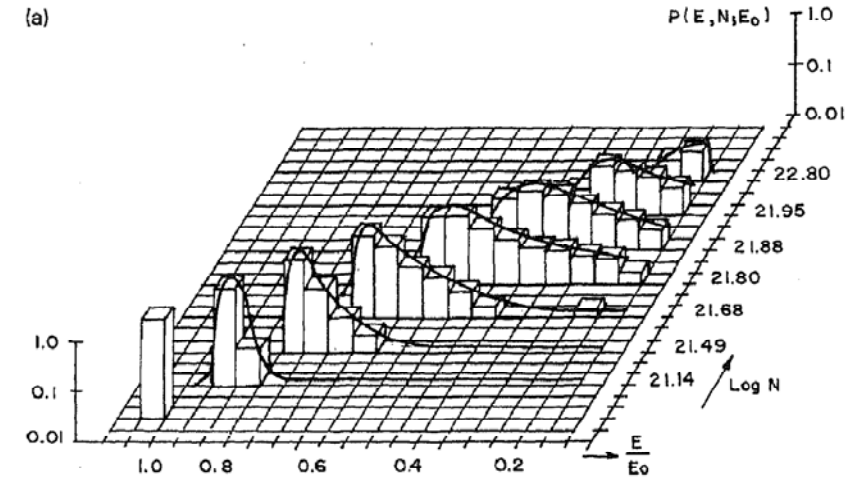


**Figure 1(a).** Variation of electron energy distribution with column density (no. of Protons $cm^{-2}$).

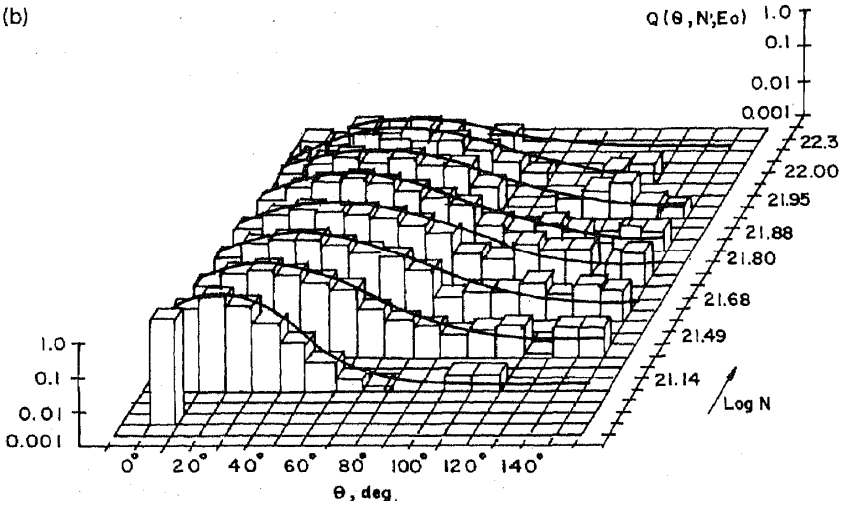


**Figure l(b).** Variation of electron angular distribution with column density (the initial electron energy is 300 keV incident at 60°).

where

$$G = \tfrac{1}{2}[[E(S)]^2/E(S) + mc^2 - 4\pi r_0^2 \ln(\theta_L/\theta_{\min})N(l, s, \cos\Theta_i)]$$

and the new polar angle $\Theta_{i+1}$ is related to the initial angle by the relation

$$\cos\Theta_{i+1} = \cos\theta\cos\Theta_i + \sin\Theta_i \cdot \sin\theta\cos\phi, \tag{10}$$

where $\phi$ is the azimuthal deflection angle which is randomly distributed between 0 and $2\pi$. The new azimuth angle $\phi_{i+1}$ is determined by

$$\sin(\phi_{i+1} - \phi_i) = \sin\phi\frac{\sin\theta}{\sin\Theta_{i+1}}. \tag{11}$$

During the following single collision of the electron with the ambient electron or proton with scattering angle $\theta_L$ and $\theta_{max}$ the electron again loses energy and changes its direction. Another random number is selected and is used to determine the scattering angle $\theta$ from the distribution

$$D(\theta, E) = \frac{\int_{\theta_L}^{\theta} \left(\frac{d\sigma}{d\theta}\right) d\theta}{\int_{\theta_L}^{\theta_{max}} \left(\frac{d\sigma}{d\theta}\right) d\theta} \tag{12}$$

is normalized to 1. The new polar and azimuth angle obtained after single collisions are again determined according to equations (10) and (11). If in an $e - e$ collision, the energy of knock on electron exceeds the threshold $E_{min} = E_0/20$ this is taken into account in the distribution function of the level $(S + l \cos \Theta_i)$. The energies of the two electrons are given by $E_1 = E - \Delta E$ and $E2 = \Delta E$. The angle $\theta$ of the knock on electron is calculated from the relativistic formula

$$\tan\theta' = \frac{2}{(\gamma + 1)\tan\theta} . \tag{13}$$

However the energy losses caused by $e - p$ collision are negligible.

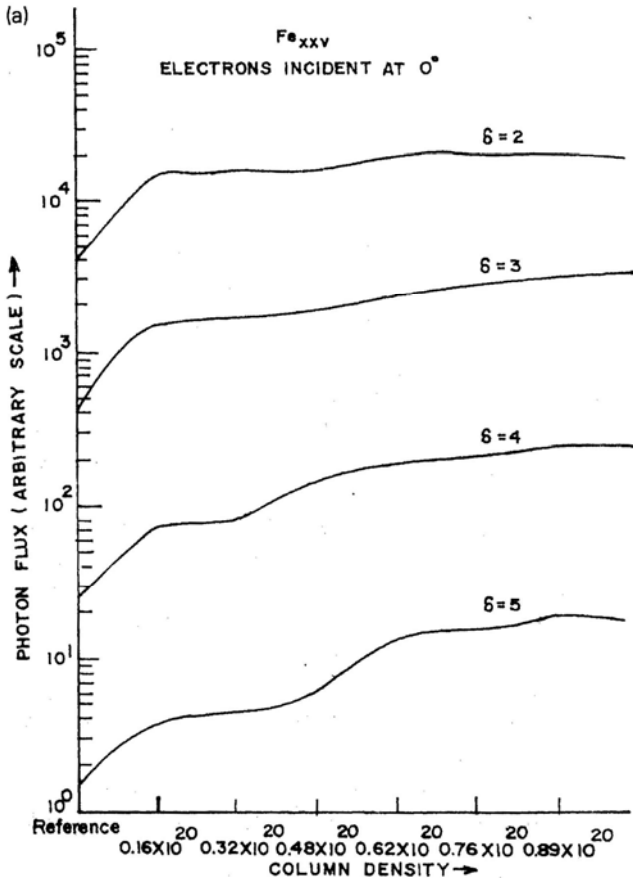


**Figure 2(a).** Variation of $F_{kl}$ for $Fe_{xxv}$ with column density for different values of electron spectral index. The incidence angle is 0°.

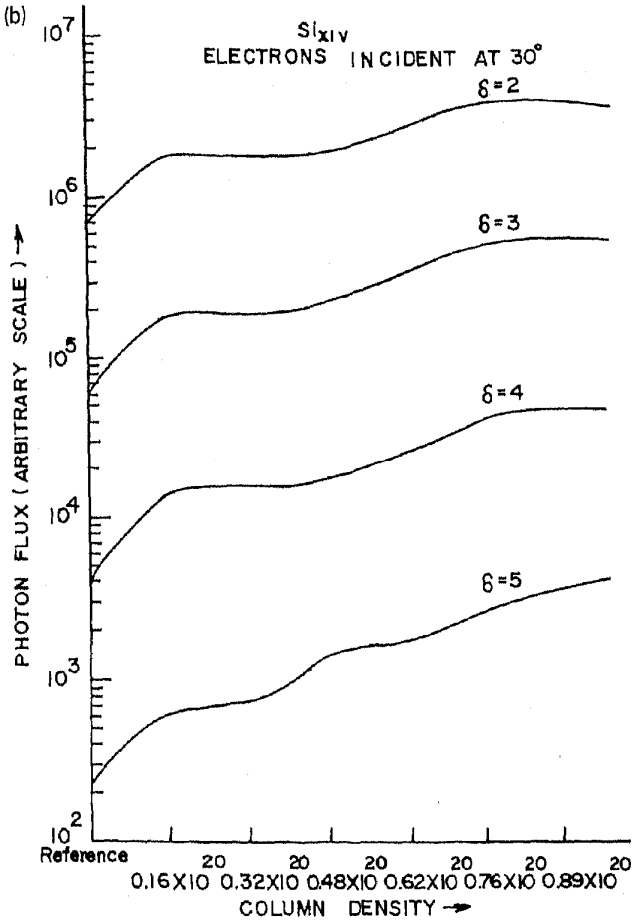


**Figure 2(b).** Same as Fig. 2(a) but for $Si_{xiv}$ and electron incidence angle is 30°.

The variation of electron energy and angular distributions are given in Figs. 1(a, b). We also find that the electrons coming at 60° are stopped at higher heights (lower column density) and electrons with 0° incidence are stopped at lower heights (higher column density) (Koul *et al* 1985). However the general trend of energy and angular distributions remains the same, becoming broad with the increase in the depth of penetration for all the incidence angles and energies of electrons (Koul *et al* 1985; Haug *et al* 1985). The number of back scattered electrons, however, increase for higher incidence angles.

## 3. X-ray and EUV line flux and EUV rise time

We have considered $Si_{xiv}$ and $Fe_{xxv}$ for the calculation of X-ray and EUV flux. For such highly ionized atoms, it is sufficient to evaluate the strength of an emission line in a two level approximation including the ground and the excited level i.e. neglecting cascades via energetically higher configurations low and intermediate energy. Therefore we follow the reasoning given by Haug (1979) that the ionization equilibrium of the coronal plasma is established predominantly by thermal processes

and is not much influenced by direct ionization due to nonthermal electrons. The flux of line photons is given by Haug 1979 as

$$F_{kl} = \frac{a_0^2}{4R^2}\frac{I_H}{g_k}B_{lk}\varepsilon_i\frac{N_{iz}}{N_i}(N_H AV)E_{kl}^{-\delta}\langle\Omega_{kl}\rangle \tag{14}$$

where the symbols have the same meaning as in Haug (1979). Haug (1979) has further shown that the same expression is valid also for thick target geometry.

Using equation (14) and the electron energy distributions calculated by the method described in section (2) we have studied the line flux $F_{kl}$ as a function of column density. The variation of the flux $F_{kl}$ with column density for different values of $\delta$ are plotted in Figs. 2(a, b). From the figures we notice that contribution to line flux $F_{kl}$ comes from the higher column density. This shows that the initial contribution of nonthermal electrons to the production of soft X-ray and EUV lines is negligible. After a few collisions, the energy distribution becomes broader and all the energies

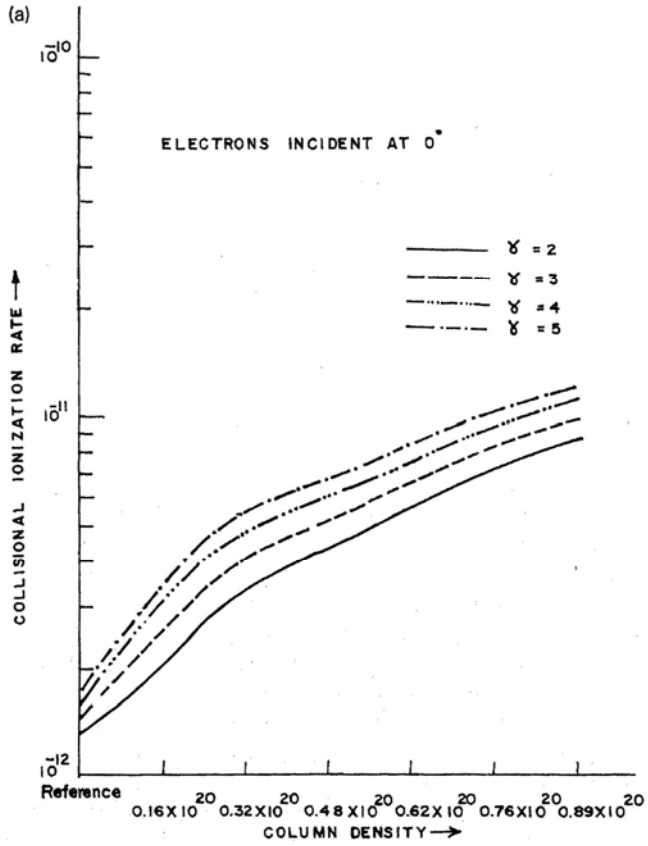


**Figure 3(a).** Variation of collisional ionization rate with column density. The electron incidence angle is 0°.

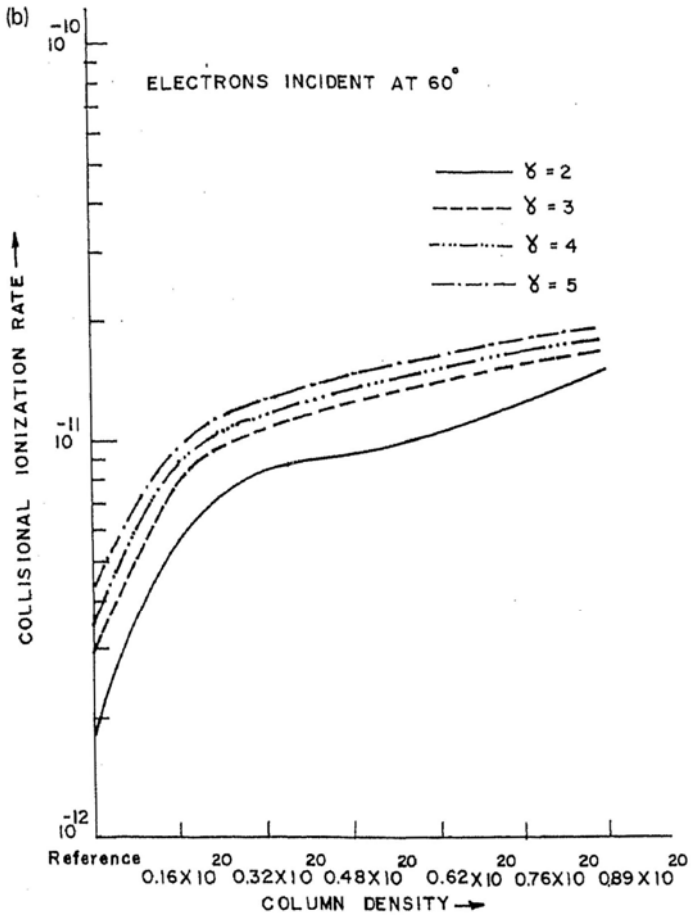


**Figure 3(b).** Same as Fig. 4(a) but for 30° electron incidence angle.

start contributing to the production of $F_{kl}$. As a result, $F_{kl}$ increases faster compared to the value of initial column density. The nature of curves, however, remains the same in case of $Si_{xiv}$ and $Fe_{xxv}$. The electron energy distributions of a monoenergetic electron beam tend towards Maxwellian by the time it reaches stopping column density. As noted earlier, the maximum contribution to line production comes from the layers close to the stopping column density at which the nature of the electron distribution is still non-Maxwellian. This means that the nonthermal component contributes significantly to the X-ray and EUV line production in flares (Bakaya *et al.* 1988). To check the validity of our calculations, we have compared the line flux with the OSO-5 observation. Our calculated values are well in agreement with the observations at discrete values. The measurement of line flux as a function of time has been carried out by Doschek *et al* (1980) and Antonucci *et al.* (1982). These experiments show that line flux increases with time and attains a maximum value and afterwards it decreases. The trend of our curves with height is almost the same. If we convert the column density traversed by the electrons into time, it will take the electron a fraction of a second to traverse the stopping column density. However the observations are for a longer duration. This means that one has to assume continuous

injection of electron beam for the explanation of time development of line profile at soft X-ray wavelengths.

Line flux due to collisional ionization also has been studied. To compute collisional ionization rate from a *z*-times ionized atom, the atomic cross-section given by Noci *et al.* (1971) has been used

$$\sigma_{\text{coll}} = A\zeta\left(\frac{I_{\text{H}}}{I_{\text{Z}}}\right)^2 \frac{I_Z}{E}\left[1 - e^{-\beta(E-I_z)/I_z}\right]\pi a_0^2 \text{cm}^2,$$

where $I_z$ is the ionization potential of the $X^{+z}$ ion, $I_H$ the hydrogen ionization potential and $\zeta$ the number of electrons in the shell from which ionization takes place. The collisional ionization rate is given by

$$q_{\text{coll}} = \left(\frac{2}{m}\right)^{\frac{1}{2}} \int_{\max(E_1, I_z)}^{\infty} E^{\frac{1}{2}} \sigma_{\text{coll}} f(E)\, \text{d}E$$

where $f(E)\text{d}E$ is the normalized distribution function for electron energies considering all energies in keV, we get

$$q_{\text{coll}} = 2.75 * 10^{-10}(\gamma - 1)\frac{\zeta}{E_1^{-\frac{1}{2}} I_z}\left[\frac{1}{\gamma - \frac{1}{2}} - 1.197\theta_{\gamma+\frac{1}{2}}\left(0.18\frac{E}{I_z}\right)\right] \text{cm}^3\,\text{s}^{-1}, \qquad (15)$$

where $\theta_{\gamma+½}$ $(X)$ is the exponential integral function $(\gamma + ½)$order. Using the above expression we have studied the line flux due to collisional ionization as function of spectral index and column density for different incidence angles shown in

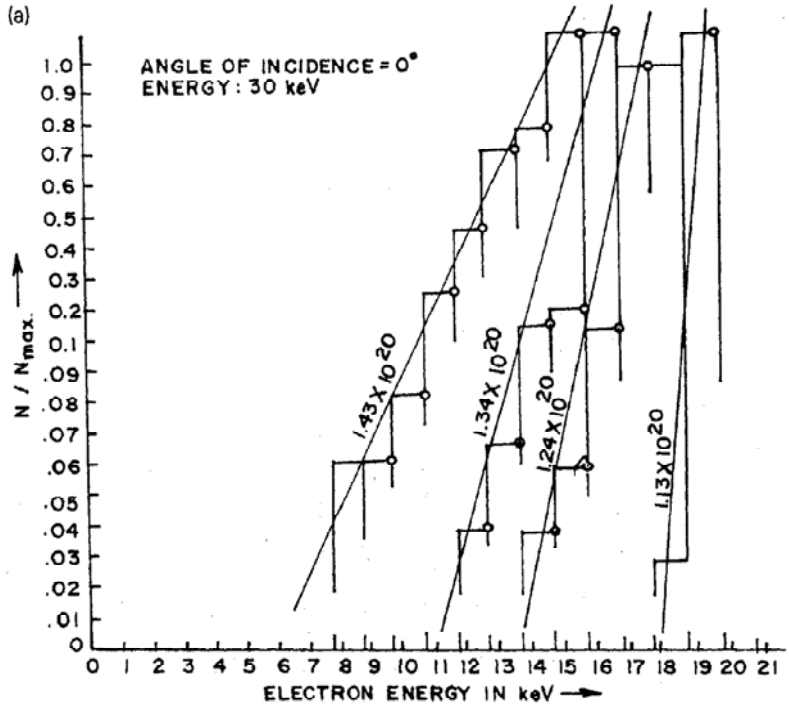


**Figure 4** (*continued*).

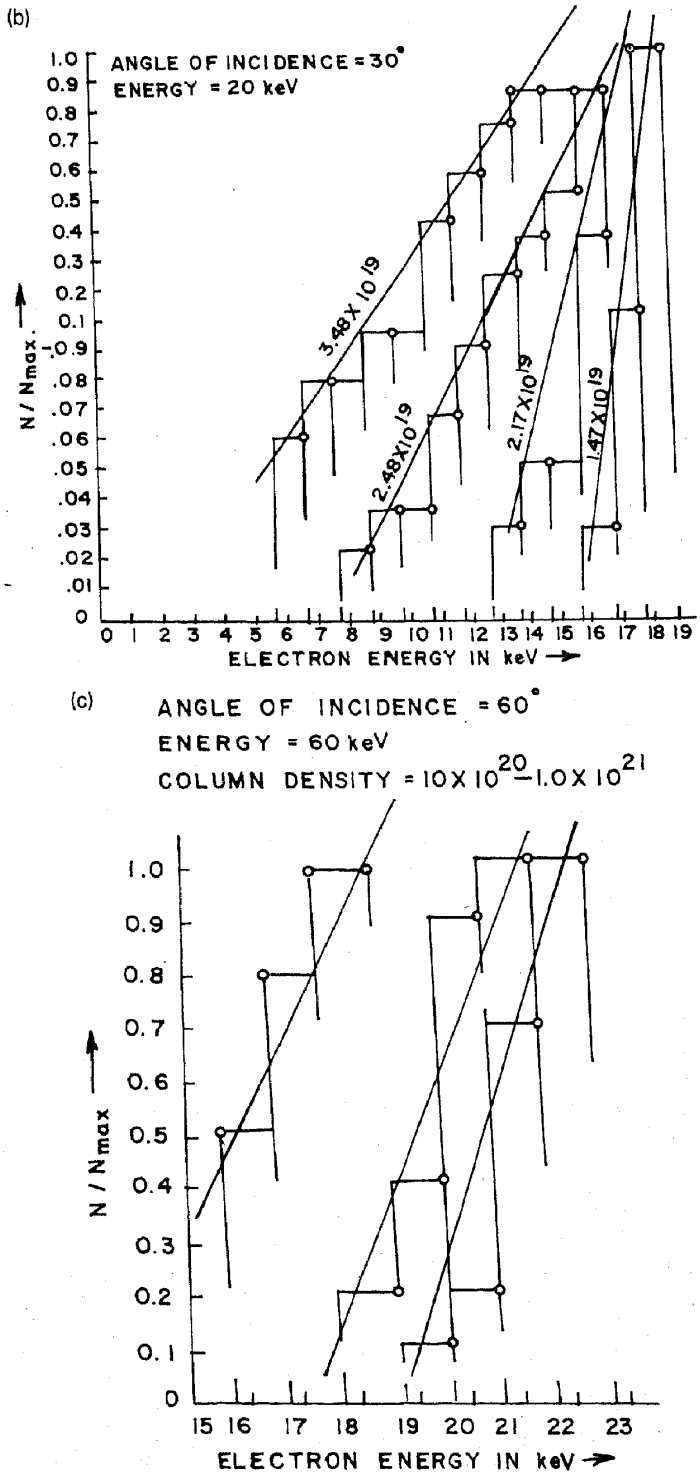


**Figure 4(a, b and c).** Variation of electron spectral index for different column densities. The initial electron energies are 20 keV, 30 keV and 60 keV incident at 0°, 30° and 60°.

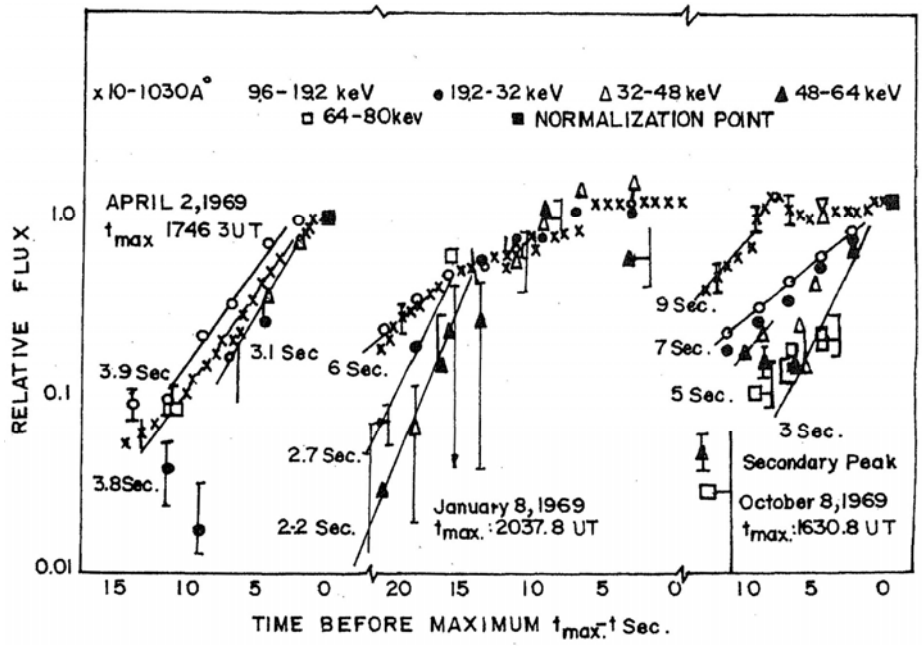


**Figure 5.** Impulsive solar EUV and hard X-ray bursts rise-time comparison.

Figs. 3(a, b). The collisional ionization rate remains almost constant as a function of electron spectral index. However it increases with the increase of column density showing that the maximum contribution to collisional ionization comes from electrons near the stopping column density.

## 4. Rise times

The rise of EUV emission is compared with the rise of hard X-ray emission for the various energy bands of the OGO-5 measurements of three flares in Figs. 4(a, b, c) where the EUV fluxes were corrected by remaining preflare background. The rise of impulsive EUV emission was found to be usually similar to that of the (9.6–19) keV X-rays. In some flares, this close agreement extended to the 19.2-32 keV X-rays, while in other bursts, the rise of EUV emission was slower than that in hard X-rays for energy bands greater than 32 keV (Bakaya *et al.* 1987). These results are independent of the small uncertainty in the EUV rise resulting from uncertainties in the ionospheric electron loss rates involved in the analysis of each particular SFD. The fact that impulsive EUV emission rises and decays slower than the X-rays above 32 keV should not be interpreted to mean that these EUV emissions are like the slow flare emissions observed at soft X-ray and EUV wavelengths. The rise times for the impulsive bursts discussed above range from several seconds to several tens of seconds, while the time constants for the slow soft X-ray and EUV emissions are typically several minutes for rise times and up to several tens of minutes for decay times. Using the electron distribution we have studied the rise times of EUV bursts. A look at the observed time profiles of EUV (Fig. 5) shows that it is steeper in the beginning and becomes flatter afterwards.

To explain this we have taken electron energy distributions in a fixed energy interval with initial electron energies of 20 keV, 30 keV and 60 keV as function of height. By taking slopes of energy distributions we find that it has the same trend as the observed one. This can be explained theoretically using the fact that in the beginning, the number of low energy electrons is smaller and it increases with the increase in column density. With the increase of low energy electrons at higher column density, the curves become flatter. The same results are obtained over a range of electron and proton energies. However the calculations are found to be sensitive to the choice of density models. A beam of high energy electrons injected towards the photosphere will be absorbed in a fraction of a second. However we find that rise times are often of the order of a few seconds. There can be two possibilities. First the electrons coming at higher incidence angles will remain trapped and will keep moving between the two conjugate points. The second possibility is that there is continuous injection of the electron beams. The second possibility seems to be more reasonable. Our calculations of hard X-ray and EUV rise times carried out so far favour nonthermal and thick target contribution.

## 5. Summary and Conclusions

We have considered a monoenergetic beam of electrons directed towards the chromosphere and have studied the evolution of electron energy and angular distributions as a function of column density. Using these distributions, characteristics of X-ray and EUV line emission and EUV rise times have been computed and compared with observations. Our calculations support X-ray and EUV line emission at higher column density (low altitudes), showing the importance of beamed thick target model. Our calculations show that the dynamical interactions of the electrons influence the characteristics of hard X-rays to a large extent. Klein *et al.* (1986) have detected a preflare phase by studying the hard X-ray emission rather than the times of the highest counting rates that are usually emphasized. They argue that peak flux depends not only on the energization process but also on dynamical evolution of the particles. Our results are consistent with the above arguments. In conclusion we say that non-thermal processes play an important role on EUV and hard X-ray characteristics which in turn are dependent on dynamical electron interaction and acceleration processes.

## Acknowledgement

We are thankful to Dr. K. K. Mahajan, Head, Radio Science Division for useful discussions and constant encouragement. Dr. Ranjna Bakaya receiving financial support from DST grant No. SR/OY/P- 03/93 is highly acknowledged.

## References

Antonucci, E. *et al.* 1982, *Sol. Phys.*, **78**, 107.
Bakaya, R., Peshin, S., Rausaria, R. R., Khosa, P. N. 1987, *J. Astrophys. Astr.*, **8**, 263.
Bakaya, R., Rausaria, R. R., Khosa, P. N. 1988, *Astrophys. Space Sci.*, **148,** 75.

Batchelor, D. A., Cranell, C. J., Wiechl, H. J., Magnum, A. 1985, *Astrophys. J.*, **195**, 258.
Batchelor, D. 1989, *Astrophys. J.*, **340**, 607.
Batchelor, D. 1990, *Astrophys. J.*, **73**, 131.
Benka, S. G., Holman, G. D. 1994, *Astrophys. J.*, **435**, 469.
Bethe, H. A. 1953, *Phys. Rev.*, **89**, 1256.
Berger, M. J. 1963, *Methods in Computation Physics*, **I**, (Academic Press) p 135.
Bohme, A., *et al.* 1977, *Sol. Phys.*, **53**, 139.
Brown, J. C. 1973, *Sol. Phys.*, **31**, 143.
Cheng, C. C. 1972, *Sol. Phys.*, **22**, 178.
Cheng, C. C. 1990, *Astrophys. J.*, **349**, 362.
Davis, D. H. 1963, *Methods in Computation Phys.*, **I**, (Academic Press) p. 67.
Doschek, G. A., Feldman, U., Kreplin, R. W., Cohen, L. 1980, *Astrophys. J.*, **239**, 725.
Duijveman, A., Somov, B. V., Spektor, A. R. 1983, *Sol. Phys.*, **88**, 257.
Elwert, G., Rausaria, R. R. 1978, *Sol. Phys.*, **57**, 409.
Emslie, A. G. 1983, *Sol. Phys.*, **86**, 133.
Emslie, A. G. 1978, *Astrophys. J.*, **224**, 241.
Emslie, A. G., Coffey, V. N., Schwartz, R. A. 1989, *Sol. Phys.*, **122**, 313.
Feldman, U., Hiel, E., Philips, K., J. H., Brown, C. M., Lang, J. 1994, *Astrophys. J.*, **421**, 483.
Giachetti, R., Pallavicini, R. 1976, *Astr. Astrophys.*, **53**, 347.
Hamilton, R. J., Petrosian, V. 1992, *Astrophys. J.*, **398**, 350.
Hammersley, J. M., Handscomb, D. C. 1964, *Monte Carlo Methods*, (New York: John Wiley & Sons Ltd.) p 40.
Haug, E. 1979, *Sol. Phys.*, **61**, 129.
Haug, E., Elwert, G., Rausaria, R. R. 1985, *Astr. Astrophys.*, **146**, 159.
Holman, G. D., Kundu, M. R., Kane, S. R. 1989. *Astrophys. J.*, **345**, 1050.
Hoyang *et al.* 1981, *Astrophys. J.*, **246**, 155.
Hudson, H. S. *et al.*. 1994, *Astrophys. J.*, **422**, L25.
Kane, S. R. *et al.* 1979, *Astrophys. J.*, **L151**, 233.
Klein, K. L., Trottet, G., Magnum, A. 1986, *Sol. Phys.* **104**, 243.
Klein, K. L., Pick, M., Magun, A., Dennis, B. R. 1987, *Sol. Phys.*, **111**, 225.
Koul, P. K., Moza K. L., Rausaria, R. R., Khosa, P. N. 1985, *Ap. J.*, **292**, 725.
Landini, M., Monsugnori Fossi, B. C., Pallavicini, R. 1973, *Sol. Phys.*, **27**, 164.
Lin, R. P., Schwartz, R. A., Pelling, R. M., Hurley, K. C. 1981, *Astrophys. J.*, **251**, L109.
Lin, R. R., Johns Christopher, M. 1993, *Astrophys. J.*, **417**, L53.
Macneice, P., McWhirter, P., Spicer, D. S., Burger, A. 1984, *Sol. Phys.*, **90**, 357.
Meekins, J. F. *et al.* 1970, *Sol. Phys.*, **16**, 465.
Moliere, G. 1948, *Zeitschrift Nature* **f 3a**, 78.
Mott, N. F., Massey, H. S. W. 1965, *Theory of Atomic Collisions* (Oxford: Clarendon Press).
Neupert, W. M. 1971, *Sol. Phys.* **18**, 474.
Noci, C. G., Chautu, A. M., Chiuderi Dargo, F. G., Grifoni Mantellini, L. A. 1971, Contract AF 61(052) 67. C0042 *Arcetri Astrophys. Obs.*
Peter, T., Ragozin, E. N., Urnov, A. M., Usko, D. B., Rust, D. M. 1990, *Astrophys. J.*, **351**, 317.
Roy, R. R., Reed, R. D. 1968, *Interaction of Photons and Leptons with Matter*, (New York, London: Academic Press).
Syrovatski, S. I., Schmeleva, C. P. 1972, *Astr. Astrophys.*, **26**, 49, 334.
Wilson, R. F., Kerdraon, A., Trottet, G., Lang, K. R. 1990, *Ap. J.*, (submitted).